Case Studies in Thermal Engineering 54 (2024) 104027

Contents lists available at ScienceDirect

Case Studies in Thermal Engineering

journal homepage: www.elsevier.com/locate/csite

Performance analysis of ocean thermal energy conversion system integrated with waste heat recovery from offshore oil and gas platform

Yanlian Du[a,b], Hao Peng[a,c,*], Jiahua Xu[d], Zhen Tian[d], Yuan Zhang[d], Xuanhe Han[e], Yijun Shen[a,c,**]

[a] State Key Laboratory of Marine Resource Utilization in South China Sea, Hainan University, Haikou, 570228, China
[b] School of Information and Communication Engineering, Hainan University, Haikou, 570228, China
[c] School of Marine Science and Engineering, Hainan University, Haikou, 570228, China
[d] Merchant Marine College, Shanghai Maritime University, Shanghai, 201306, China
[e] Mechanical and Electrical Engineering College, Hainan University, Haikou, 570228, China

HIGHLIGHTS

- Waste heat from offshore oil and gas platform is used to improve OTEC efficiency.
- Four systems are designed to utilize flue gas and production water waste heat.
- Thermodynamic model for predicting the novel system performance is established.
- Power generation, thermal efficiency and exergy efficiency are increased.

ARTICLE INFO

Keywords:
Flue gas
Ocean thermal energy conversion
Production water
Thermodynamic performance
Waste heat recovery

ABSTRACT

To improve ocean thermal energy conversion (OTEC) system efficiency, four systems utilizing the waste heat recovery from offshore oil and gas platform are proposed, including flue gas boosting OTEC (system I), production water boosting surface seawater OTEC (system II), production water boosting working medium OTEC (system III), and production water boosting vapor OTEC (system IV). The system thermodynamic performance are investigated. The results show that system IV has larger power generation (W_{net}), thermal efficiency (η_{th}) and exergy efficiency (η_{ex}) than others. Compared with single OTEC system, for system IV, W_{net}, η_{th} and η_{ex} are increased by 1569.13 %, 70.35 % and 138.26 %, respectively. For system IV, with the increase of flue gas waste heat quantity from 2000 to 4000 kW, W_{net}, η_{th} and η_{ex} are increased by 562 %, 390 % and 181 % respectively; with the increase of production water waste heat quantity from 0 to 100 kW, W_{net}, η_{th} and η_{ex} are 12.59 %, 5.73 % and 2.86 % respectively. W_{net} rises first and then decreases with the increase of evaporation pressure (P_{eva}) or base fluid concentration (x_b), presenting an optimal P_{eva} of 1.5 MPa and x_b of 0.82 corresponding to the maximum W_{net}; W_{net} decreases with the increase of condensation temperature.

* Corresponding author. State Key Laboratory of Marine Resource Utilization in South China Sea, Hainan University, Haikou, 570228, China.
** Corresponding author. State Key Laboratory of Marine Resource Utilization in South China Sea, Hainan University, Haikou, 570228, China.
E-mail addresses: 996027@hainanu.edu.cn (H. Peng), sheny2000@hainanu.edu.cn (Y. Shen).

https://doi.org/10.1016/j.csite.2024.104027
Received 3 December 2023; Received in revised form 11 January 2024; Accepted 12 January 2024
Available online 13 January 2024

Nomenclature

c	specific heat ($J{\cdot}kg^{-1}{\cdot}k^{-1}$)
D	equivalent diameter (m)
$\dot{E}$	exergy (W)
g	gravity acceleration ($m{\cdot}s^{-2}$)
h	specific enthalpy ($J{\cdot}kg^{-1}$)
ΔP	pressure drop (Pa)
$\dot{E}_D$	exergy destruction (W)
L	length (m)
P	pressure (Pa)
$\dot{m}$	mass flow rate ($kg{\cdot}s^{-1}$)
$\dot{Q}$	heat quantity (W)
s	specific entropy ($J{\cdot}kg^{-1}{\cdot}k^{-1}$)
T	temperature (°C)
V	flow velocity ($m{\cdot}s^{-1}$)
W	power, work (W)
x	ammonia concentration (–)

Greek symbols

ρ	density ($kg{\cdot}m^{-3}$)
η	efficiency (–)

Subscripts

a	ambient
b	ammonia-water mixture base fluid
con	condenser
c	deep cold seawater
cp	deep cold seawater pump
eva	evaporation
fg	flue gas
hw	high- temperature production water
i	state point
in	inlet, input
l	lean ammonia solution
mix	mixer
opt	optimal
out	outlet
p	pump
reg	regenerator
sep	separator
th	thermal
total	total
tur	turbine
v	ammonia vapor
val	throttle valve
w	surface warm seawater
wp	surface warm seawater pump

Abbreviation

LNG	liquefied natural gas
NH_3–H_2O	Ammonia-water
ORC	organic Rankine cycle
OTEC	ocean thermal energy conversion
PEM	proton exchange membrane
WHROG	waste heat recovery from offshore oil and gas platform

1. Introduction

Ocean thermal energy is a promising clean and renewable energy, which has high stability, small periodic fluctuations and large reserves [1–4]. Ocean thermal energy conversion (OTEC) is estimated to have the annual power production capacity of 30 TW [5]. During OTEC system operation, the working medium is vaporized to drive a steam turbine to generate power; after completing the work, the exhaust steam is condensed to liquid state by deep seawater, and then transported by the working medium pump to the evaporator for further vaporization. However, single OTEC system is faced with a critical issue of low efficiency and small power generation, which is caused by the relatively low temperature difference between surface and deep seawater [6,7]. In order to meet the actual power demand, the temperature difference between heat and cold sources of OTEC system should be increased.

Waste heat recovery can be used to increase the heat source temperature of thermodynamic cycle and then improve the cycle efficiency [8–12]. During the operation of offshore oil and gas platform, high-temperature flue gas and production water carry a large amount of waste heat. For example, about 30 % of heat energy in gas turbine power plant of offshore oil and gas platform is directly discharged into the atmosphere, and the flue gas temperature can exceed 400 °C. During the oil extraction process, due to the high temperature of stratum and the heating process for reducing crude oil viscosity, the temperature of production water can reach 110 °C. Therefore, the waste heat recovery from offshore oil and gas platform has great potential for improving OTEC system performance.

The existing researches for improving OTEC system performance can be divided into two categories, one is the improvement of cycle design and working medium selection, the other is the combination between OTEC with other clean energy sources. For the improvement of cycle design and working medium selection, Kalina [13] proposed Kalina cycle using non azeotropic working medium; the temperature slip existing for non azeotropic working medium can reduce irreversible loss during phase transition process [14–17], and the presence of separator can reduce the power consumption of surface warm seawater pump. Due to the small temperature difference between surface and deep seawater, the heat recovery effect of regenerator in Kalina cycle was not significant. For solving this issue, Uehara cycle was proposed [18]; the heat from lean ammonia solution was collected and some of turbine exhaust steam was extracted for preheating base liquid, resulting in higher thermal efficiency than Kalina cycle.

Liu et al. [19] have proposed a novel closed OTEC cycle. In the cycle, the base liquid is preheated with lean ammonia solution, and then a portion of turbine exhaust steam was extracted for secondary preheating of base liquid. The system efficiency is 64.5 % and 2.6 % higher than those of Rankine cycle and Uehara cycle, respectively.

Yoon et al. [20] have proposed a high-efficiency R717 OTEC cycle with an expansion valve and a cooler. The system includes two steam turbines and two regenerators, which are used to increase the power generation and preheat the base liquid respectively. The system efficiency is 0.9 % and 1.7 % higher than those of Uehara cycle and Kalina cycle, respectively.

Yuan et al. [21] have proposed an OTEC system with two ejectors. The ammonia-water mixture is adopted as working fluid, and the ejectors are driven by vapor and solution from sub-generator. The absorption temperature is increased by 2.0–6.5 °C, indicating that the proposed cycle can be driven with a lower temperature difference. The thermal efficiency, net thermal efficiency and exergy efficiency can reach 4.17 %, 3.10 % and 39.92 % respectively.

Kusuda et al. [22] have proposed an OTEC system with double-stage Rankine cycle. Compared with single-stage Rankine cycle, the entropy generation rate is reduced, and the output power is increased.

Yoon et al. [23] have proposed an OTEC system with a liquid-vapor ejector and a motive pump. With the application of the liquid-vapor ejector, the turbine outlet pressure becomes lower than that in basic OTEC. The system efficiency can reach 4.0 %, which is 38 % higher than that of basic OTEC.

Wu et al. [24] have established a constructal thermodynamic optimization model for OTEC system with a dual-pressure organic Rankine cycle. The combination of constructal theory with finite time thermodynamics is used. The net power output after optimization can be improved by 14.95 %.

Kim et al. [25] have compared the thermodynamic performance of different OTEC cycles including simple Rankine cycle, regenerative Rankine cycle, Kalina cycle, open cycle and hybrid cycle. Compared with simple Rankine cycle, the energy efficiencies of regenerative Rankine cycle and Kalina cycle are increased by 1.5 %–2 % and 2 %–3 % respectively, and the overall cycle efficiencies of hybrid cycle and open cycle are 3.35 % and 4.86 % respectively.

For the combination between OTEC with other clean energy sources, Kim et al. [26] have used condenser effluent from a nuclear power plant as the heat source for OTEC. Compared with the system only using surface seawater, the thermal efficiency is increased by at least 2 %.

Yamada et al. [27] have proposed solar-boosted OTEC system, in which the temperature of warm seawater is boosted by a typical low-cost solar thermal collector. The annual mean net thermal efficiency is approximately 1.5 times higher than that of conventional OTEC plant if a single-glazed flat-plate solar collector with 5000 m^2 effective area is installed to boost the surface seawater temperature by 20 K.

Aydin et al. [3] have designed a OTEC system with a solar thermal collector integrated as an add-on preheater or superheater. For both preheating and superheating cases, the net power generation are increased by 20 %–25 %. For superheating case, the system thermal efficiency is increased from 1.9 % to 3 %.

Ahmadi et al. [28] have proposed an OTEC system coupled with a solar-enhanced proton exchange membrane (PEM) electrolyzer. The energy and exergy efficiencies of the integrated OTEC system are 3.6 % and 22.7 % respectively, and the exergy efficiency of the PEM electrolyzer is about 56.5 % while the amount of hydrogen production is 1.2 kg h^{-1}.

Arcuri et al. [29] have proposed an OTEC system using liquefied natural gas (LNG) as cold source. The system efficiency can reach 17.5 % when LNG temperature at the inlet of condenser is −160 °C.

Idrus et al. [30] have proposed an OTEC system combined with geothermal energy. The system produces different net power outputs with various superheated ammonia temperatures at fixed geothermal energy input. The system thermal efficiency can reach 4.61 %.

Yilmaz [31] has proposed a new wind-OTEC hybrid plant for clean power production. The system consists of two main sub-cycles, including working fluid OTEC system and wind turbine. The overall energy and exergy efficiencies of the hybrid system are 12.27 % and 23.34 %, respectively.

Yilmaz et al. [32] has proposed a new OTEC based hydrogen production and liquefaction system. The solar collector is integrated with OTEC system. The energy and exergy efficiencies of integrated system are founded to be 43.49 % and 36.49 %, respectively.

The existing researches on waste heat recovery from offshore oil and gas platform are mainly concerned with Brayton cycle [33], organic Rankine cycle (ORC) [34–37], air bottoming cycle [37,38] and steam Rankine cycle [37]. Liu et al. [33] have investigated the thermal performance of Brayton cycle with waste heat recovery boiler for diesel engines in offshore oil production facilities. With the utilization of waste heat recovery boiler instead of thermal boiler, the system energy efficiency without fan is slightly reduced but heat recovery efficiency is improved.

Reis et al. [34] have conducted the off-design performance analysis and optimization of power production by ORC coupled with gas turbine in offshore oil platform. The ORC is very flexible in the heat recovery under dynamic demand conditions, contributing up to 20.3 % in electricity generation, which causes an increase in overall system efficiency of up to 11.3 %.

Pierobon et al. [35] have performed the multi-objective optimization of ORC for waste heat recovery from gas turbine in off-shore oil and gas platform. For working fluid of acetone, the thermal efficiency ranges from 23.7 % to 27.0 %. For working fluid of cyclopentane, the thermal efficiency ranges from 27.0 % to 28.1 %.

Nami et al. [36] have proposed gas turbine exhaust heat recovery by ORC to supply energy offshore. Two configurations (cascade and series) are proposed. Siloxane MM and R124 are the best working fluids for the cascade and series systems. Decreasing the ORC minimum pressure in the series system makes considerable improvement.

Pierobon et al. [37] have utilized multi-objective design-point optimization to compare ORC, air bottoming cycle and steam Rankine cycle for waste heat recovery from gas turbine in offshore oil and gas platform. ORC presents larger performance compared with steam Rankine cycle, and the implementation of air bottoming cycle is not attractive from economic and environmental perspective compared with other two cycles.

Pierobon and Haglind [38] have design an air bottoming cycle to recover the waste heat from gas turbine in offshore platform. Through the theory of power maximization, the power of gas turbine and thermal efficiency can be increased by 16 % and 5.2 %, respectively.

From the literature review, it can be seen that the research on OTEC system integrated with waste heat recovery from offshore oil and gas platform is rarely reported. The purpose of this study to present a novel OTEC system integrated with waste heat recovery from offshore oil and gas platform (OTEC-WHROG). The effects of flue gas waste heat quantity, production water waste heat quantity, evaporation pressure, base fluid concentration and condensation temperature on system performance are investigated, and compared with single OTEC system. The novelty of this study includes: (1) waste heat recovery from offshore oil and gas platform to improve OTEC system efficiency; (2) design of four heat exchange configurations for effective utilization of heat from high-temperature flue gas and production water.

2. System design

The ocean thermal energy conversion systems integrated with waste heat recovery from offshore oil and gas platform (OTEC-WHROG) are designed. According to the waste heat sources (high-temperature flue gas and production water) and heated objects, the systems can be divided into four different types, including flue gas boosting OTEC system (system I), production water boosting surface seawater OTEC system (system II), production water boosting working medium OTEC system (system III), and production water boosting vapor OTEC system (system IV).

For these four systems, Kalina cycle is adopted for OTEC. The reasons for adopting Kalina cycle are as follows: (1) Kalina cycle adopting ammonia-water mixture as working fluid can achieve variable evaporation temperature. During the evaporation process, the ammonia concentration is decreased, which leads to the increase of solution boiling point, so that the evaporation matches the heat transfer process. Consequently, the irreversible loss during heat transfer process is reduced, and the thermal efficiency is improved [14,17]. (2) The exhausted gas is adopted to heat the working fluid before passing the evaporator, which reduces the consumption of surface warm seawater. (3) Both theoretical and practical investigations reveal that the thermal efficiency of Kalina cycle is higher than that of Rankine cycle [14,17]. (4) Kalina cycle can adapt to different operation conditions by adjusting the concentration of ammonia-water mixture.

Ammonia-water (NH_3–H_2O) mixture is adopted as working medium, and has variable-temperature evaporation characteristics, which reduces the temperature difference and exergy destruction during heat transfer process. The properties of Ammonia used in the present study are listed in Table 1.

The equipment for the cycle include the evaporator, separator, steam turbine, regenerator, throttle valve, mixer, condenser, working medium pump, surface and deep seawater pumps. There are three forms of ammonia-water mixture in the cycle, including base fluid, rich ammonia vapor, and lean ammonia solution. The base liquid of ammonia-water mixture absorbs the heat from surface seawater through the evaporator; the ammonia in the mixture, which has relatively lower boiling point, is evaporated and transformed into ammonia vapor, changing the base liquid to be gas-liquid mixture (stages 1–2). The ammonia-water gas-liquid mixture is separated into rich ammonia vapor with higher ammonia concentration (stages 2–3) and lean ammonia solution with low ammonia con-

Table 1
Properties of Ammonia used in the present study.

Working medium	Chemical and physical properties				Environmental characteristics			Type
	Molar mass (g mol^{-1})	Critical temperature (°C)	Critical pressure (MPa)	Standard boiling point (°C)	GWP	ODP	Safety Group	Character
Ammonia	17.03	132.4	11.2	−33.3	0	0	B2L	Wet

centration (stages 2–5) through the separator. The rich ammonia vapor enters the steam turbine to do work and drives the generator to generate electricity (stages 3–4). Through regenerator, the lean ammonia solution preheats the base liquid of ammonia-water mixture not entering the evaporator (stages 5–6). After that, the lean ammonia solution undergoes pressure adjustment through the throttle valve (stages 6–7), and then is mixed with the steam turbine exhaust through the mixer to form the base liquid of ammonia-water mixture (stages 4, 7–8). The mixed base liquid of ammonia-water mixture is condensed to liquid phase by deep seawater through the condenser (stages 8–9), pressurized by the working medium pump (stages 9–10), preheated by the regenerator (stages 10-1), and then enters the evaporator again to complete a cycle.

For system I, the surface seawater is heated by high-temperature flue gas before entering the evaporator, as shown in Fig. 1 (a). For system II, the surface seawater is heated by high-temperature production water and flue gas before entering the evaporator, as shown in Fig. 1 (b). For system III, the surface seawater is heated by high-temperature flue gas before entering the evaporator, and the base fluid of ammonia-water mixture is heated by high-temperature production water before entering the separator (stages 11–12), as shown in Fig. 1 (c). For system IV, the surface seawater is heated by high-temperature flue gas before entering the evaporator, and the rich ammonia vapor is heated by high-temperature production water before entering the steam turbine (stages 11–12), as shown in Fig. 1 (d).

3. Thermodynamic modeling

3.1. Modeling technical route and assumptions

A thermodynamic model for OTEC-WHROG system is established, which includes three sub-models, i.e., high-temperature flue gas boosting sub-model (sub-model 1), high-temperature production water boosting sub-model (sub-model 2), and OTEC performance sub-model (sub-model 3), as shown in Fig. 2. The input parameters of overall model are: flue gas waste heat quantity, production water waste heat quantity, evaporation pressure, base fluid concentration and condensation temperature. The output parameters are: power generation, thermal efficiency, exergy efficiency, and total exergy destruction. The temperature of surface seawater at the outlet of flue gas heat exchanger is calculated through sub-model 1; the temperature of surface seawater as well as the enthalpy of working medium at the outlet of production water heat exchanger are calculated through sub-model 2; the temperature, enthalpy, evaporation pressure, base fluid concentration, and condensation temperature are used as input parameters for sub-model 3.

For the simplification of physical problem, some assumptions are made as follows: (1) the pressure drop in pipelines connecting equipment are ignored; (2) the heat losses of various components in the system are ignored; (3) the mechanical loss of steam turbine and the pressure loss of mixer are ignored; (4) the system operates under stable conditions; (5) the pressure drop in flue gas and production water heat exchangers are ignored.

3.2. High-temperature flue gas boosting sub-model

The temperature of surface warm seawater at the outlet of flue gas heat exchanger is

$$T_{\mathrm{w,fgout}} = T_{\mathrm{w,fgin}} + \frac{\dot{Q}_{\mathrm{fg}}}{\dot{m}_{\mathrm{w}} c_{\mathrm{w}}} \tag{1}$$

where $\dot{m}_{\mathrm{w}}$ is the mass flow rate of surface warm seawater, set as 15 kg s^{-1} in the present study; c_{w} is the specific heat of surface warm seawater, and has the value of 4.179 kJ kg^{-1} K^{-1}; $T_{\mathrm{w,\ fgin}}$ is the temperature of surface warm seawater at the inlet of flue gas heat exchanger, set as 298.15 K in the present study; $\dot{Q}_{\mathrm{fg}}$ is the flue gas waste heat quantity.

3.3. High-temperature production water boosting sub-model

3.3.1. Production water boosting surface seawater OTEC system

The temperature of surface warm seawater at the outlet of production water heat exchanger is

$$T_{\mathrm{w,hwout}} = T_{\mathrm{w,hwin}} + \frac{\dot{Q}_{\mathrm{hw}}}{\dot{m}_{\mathrm{w}} c_{\mathrm{w}}} \tag{2}$$

where $T_{\mathrm{w,\ hwin}}$ is the temperature of surface warm seawater at the inlet of production water heat exchanger; $\dot{Q}_{\mathrm{hw}}$ is the production water waste heat quantity.

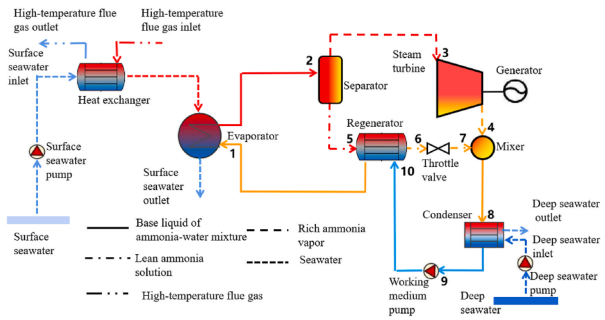

(a) Flue gas boosting OTEC system (system I)

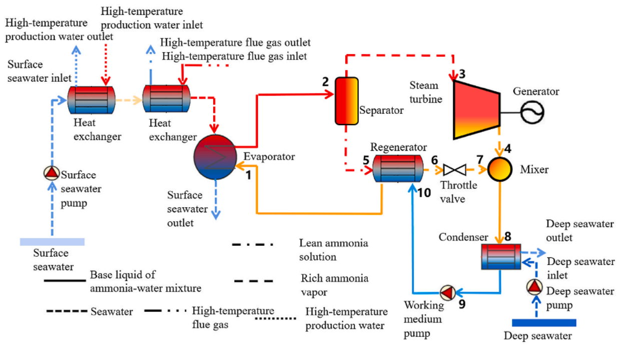

(b) Production water boosting surface seawater OTEC system (system II)

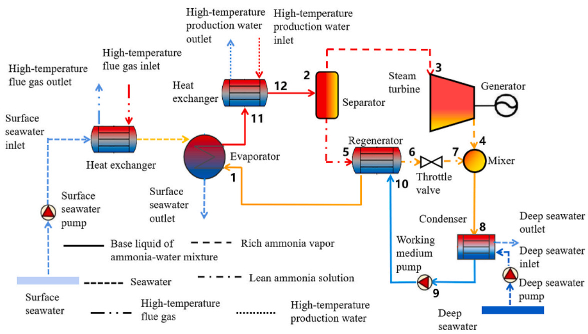

(c) Production water boosting working medium OTEC system (system III)

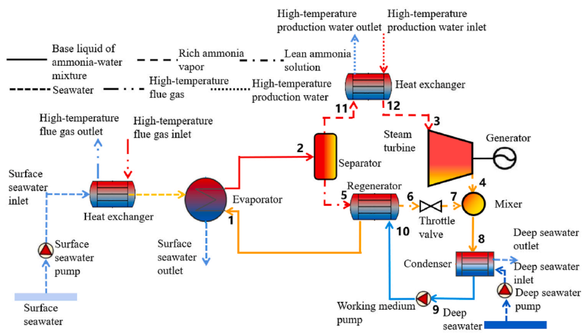

(d) Production water boosting vapor OTEC system (system IV)

Fig. 1. Schematic diagram of four different OTEC-WHROG systems.

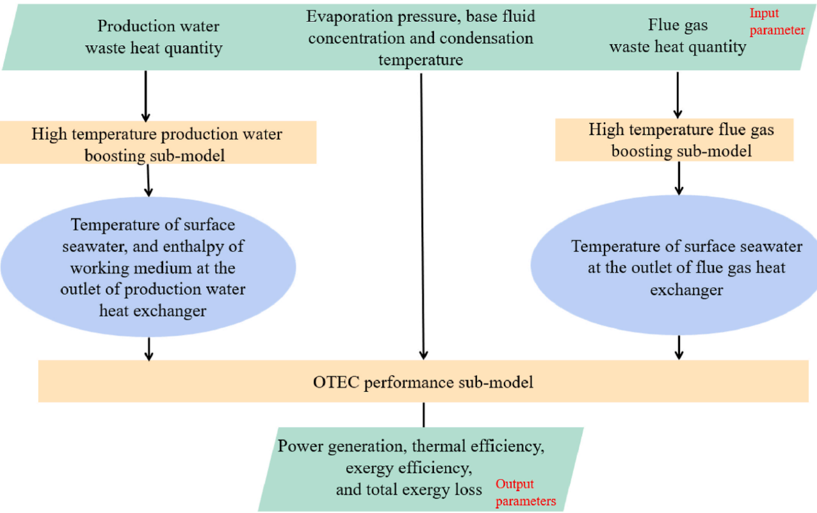

Fig. 2. Technical route of thermodynamic model for OTEC-WHROG system.

3.3.2. *Production water boosting working medium OTEC system*

The specific enthalpy of ammonia-water mixture base fluid at the outlet of production water heat exchanger is

$$h_{12} = h_{11} + \frac{\dot{Q}_{\mathrm{hw}}}{\dot{m}_{\mathrm{b}}} \tag{3}$$

where h_{11} is the specific enthalpy of ammonia-water mixture base fluid at the inlet of production water heat exchanger; $\dot{m}_{\mathrm{b}}$ is the mass flow rate of ammonia-water mixture base fluid.

3.3.3. *Production water boosting vapor OTEC system*

The specific enthalpy of rich ammonia vapor at the outlet of production water heat exchanger is

$$h_{12} = h_{11} + \frac{\dot{Q}_{\mathrm{hw}}}{\dot{m}_{\mathrm{v}}} \tag{4}$$

where h_{11} is the specific enthalpy of rich ammonia vapor at the inlet of production water heat exchanger; $\dot{m}_{\mathrm{v}}$ is the mass flow rate of rich ammonia vapor.

3.4. *OTEC performance sub-model*

3.4.1. *Energy modeling*

3.4.1.1. Evaporator. The heat exchange quantity in evaporator is calculated by

$$\dot{Q}_{\mathrm{eva}} = \dot{m}_{\mathrm{b}}\left(h_2 - h_1\right) = \left(T_{\mathrm{w,in}} - T_{\mathrm{w,out}}\right) c_{\mathrm{w}} \dot{m}_{\mathrm{w}} \tag{5}$$

where h_1 and h_2 are the specific enthalpy values of working medium at the state points 1 and 2, respectively; $T_{\mathrm{w,\ in}}$ and $T_{\mathrm{w,\ out}}$ are the temperatures of surface warm seawater at the inlet and outlet of evaporator, respectively.

Thus, there is

$$T_{\mathrm{w,out}} = T_{\mathrm{w,in}} - \frac{\dot{m}_{\mathrm{b}}\left(h_2 - h_1\right)}{c_{\mathrm{w}} \dot{m}_{\mathrm{w}}} \tag{6}$$

3.4.1.2. Separator. Energy conservation:

$$\dot{m}_{\mathrm{b}} h_2 = \dot{m}_{\mathrm{v}} h_3 + \dot{m}_{\mathrm{l}} h_5 \tag{7}$$

Ammonia mass conservation:

$$\dot{m}_{\mathrm{b}} x_2 = \dot{m}_{\mathrm{v}} x_3 + \dot{m}_{\mathrm{l}} x_5 \tag{8}$$

Working medium mass conservation:

$$\dot{m}_{\mathrm{b}} = \dot{m}_{\mathrm{l}} + \dot{m}_{\mathrm{v}} \tag{9}$$

where $\dot{m}_l$ is the mass flow rate of lean ammonia solution, respectively; h_3 and h_5 are the specific enthalpy values of working medium at the state points 3 and 5, respectively; x_2, x_3 and x_5 are the ammonia concentrations at the state points 2, 3 and 5, respectively.

3.4.1.3. Steam turbine. The isentropic efficiency of steam turbine is

$$\eta_{tur} = \frac{h_3 - h_4}{h_3 - h_{4s}} \tag{10}$$

where h_4 and h_{4s} are the actual and isentropic specific enthalpy values of working medium at the state point 4, respectively.

The isentropic expansion process is expressed as

$$s_3 = s_{4s} \tag{11}$$

where s_3 and s_{4s} are the specific and isentropic specific entropy values of working medium at the state points 3 and 4, respectively.

The expansion work is

$$W_{tur} = \dot{m}_v \left(h_3 - h_4\right) \tag{12}$$

3.4.1.4. Mixer. Energy conservation:

$$\dot{m}_b h_8 = \dot{m}_v h_4 + \dot{m}_l h_7 \tag{13}$$

Ammonia mass conservation:

$$\dot{m}_b x_8 = \dot{m}_v x_4 + \dot{m}_l x_7 \tag{14}$$

Working medium mass conservation:

$$\dot{m}_b = \dot{m}_l + \dot{m}_v \tag{15}$$

where h_7 and h_8 are the specific enthalpy values of working medium at the state points 7 and 8, respectively; x_4, x_7 and x_8 are the ammonia concentrations at the state points 4, 7 and 8, respectively.

3.4.1.5. Condenser. The heat exchange quantity in condenser is calculated by

$$\dot{Q}_{con} = \dot{m}_b \left(h_8 - h_9\right) \tag{16}$$

where h_9 is the specific enthalpy value of working medium at the state point 9.

The mass flow rate of deep cold seawater is

$$\dot{m}_c = \frac{\dot{Q}_{con}}{c_c \left(T_{c,out} - T_{c,in}\right)} \tag{17}$$

where $\dot{m}_c$ is the mass flow rate of deep cold seawater; c_c is the specific heat of deep cold seawater; $T_{c,\,in}$ and $T_{c,\,out}$ are the temperatures of deep cold seawater at the inlet and outlet of condenser, respectively.

3.4.1.6. Working medium pump. The isentropic process for working medium pump is described as

$$s_9 = s_{10} \tag{18}$$

where s_9 and s_{10} are the specific entropy values of working medium at the state points 9 and 10, respectively.

The power consumption of working medium pump is

$$W_p = \frac{\dot{m}_b \left(h_{10} - h_9\right)}{\eta_p} \tag{19}$$

where h_{10} is the specific enthalpy value of working medium at the state point 10; η_p is the efficiency of working medium pump.

3.4.1.7. Regenerator. According to energy conversion, there is

$$\dot{m}_l \left(h_6 - h_5\right) = \dot{m}_b \left(h_1 - h_{10}\right) \tag{20}$$

where h_5 and h_6 are the specific enthalpy values of working medium at the state points 5 and 6, respectively.

3.4.1.8. Throttle valve. According to energy conversion, there is

$$h_6 = h_7 \tag{21}$$

3.4.1.9. Seawater pump. The equivalent diameter of surface warm seawater pipeline is

$$D_w = \left(\frac{\dot{m}_w 4}{\rho_w V_w \pi}\right)^{0.5} \tag{22}$$

The total pressure drop of surface warm seawater in pipeline is

$$\Delta P_w = 6.82 \frac{L_w}{D_w^{1.17}} \left(\frac{V_w}{100}\right)^{1.85} + \frac{V_w^2}{g} \tag{23}$$

The power consumption of surface warm seawater pump is

$$W_{wp} = \frac{\dot{m}_w \Delta P_w g}{\eta_{wp}} \tag{24}$$

The equivalent diameter of deep cold seawater pipeline is

$$D_c = \left(\frac{\dot{m}_c 4}{\rho_c V_c \pi}\right)^{0.5} \tag{25}$$

The total pressure drop of deep cold seawater in pipeline is

$$\Delta P_c = 6.82 \frac{L_c}{D_c^{1.17}} \left(\frac{V_c}{100}\right)^{1.85} + \frac{V_c^2}{g} + \left[L_c - \frac{L_c (\rho_c + \rho_w)}{2\rho_c}\right] \tag{26}$$

The power consumption of deep cold seawater pump is

$$W_{cp} = \frac{\dot{m}_c \Delta P_c g}{\eta_{cp}} \tag{27}$$

where V_w and V_c are the flow velocities of warm and cold seawater, respectively; ρ_w and ρ_c are the densities of warm and cold seawater, respectively; L_w and L_c are the lengths of warm and cold seawater pipelines, respectively; g is gravitational acceleration with the value of 9.8 m s^{-2}; η_{wp} and η_{cp} are the efficiencies of warm and cold seawater pumps, respectively.

The system power generation is

$$W_{net} = W_{tur} - W_p - W_{wp} - W_{cp} \tag{28}$$

The thermal efficiency for flue gas boosting OTEC system is

$$\eta_{th} = \frac{W_{net}}{\dot{Q}_{eva} + \dot{Q}_{fg}} \tag{29}$$

The thermal efficiency for production water boosting OTEC system is

$$\eta_{th} = \frac{W_{net}}{\dot{Q}_{eva} + \dot{Q}_{hw}} \tag{30}$$

3.4.2. Exergy modeling

The exergy destruction of evaporator, separator, steam turbine, mixer, condenser, regenerator and throttle valve are calculated by Eq. (31) ~ (37), respectively.

$$\dot{E}_{D,eva} = T_a \left[\dot{m}_b (s_2 - s_1) - \frac{2\dot{Q}_{eva}}{T_{w,in} + T_{w,out}}\right] \tag{31}$$

$$\dot{E}_{D,sep} = T_a (\dot{m}_v s_3 + \dot{m}_l s_5 - \dot{m}_b s_2) \tag{32}$$

$$\dot{E}_{D,tur} = T_a \dot{m}_v (s_4 - s_3) \tag{33}$$

$$\dot{E}_{D,mix} = T_a (\dot{m}_b s_8 - \dot{m}_v s_4 - \dot{m}_l s_7) \tag{34}$$

$$\dot{E}_{D,con} = \dot{m}_b [(h_8 - h_9) - T_a (s_8 - s_9)] \tag{35}$$

$$\dot{E}_{\mathrm{D,reg}} = T_{\mathrm{a}}\left[\dot{m}_{\mathrm{b}}\left(s_1 - s_{10}\right) - \dot{m}_{\mathrm{l}}\left(s_6 - s_5\right)\right] \tag{36}$$

$$\dot{E}_{\mathrm{D,val}} = T_{\mathrm{a}}\dot{m}_{\mathrm{l}}\left(s_7 - s_6\right) \tag{37}$$

where T_{a} is the ambient temperature; s_1, s_2, s_4, s_5, s_6, s_7 and s_8 are the specific entropy values of working medium at the state points 1, 2, 4, 5, 6, 7 and 8, respectively.

The total exergy destruction is

$$\dot{E}_{\mathrm{D,total}} = \dot{E}_{\mathrm{D,eva}} + \dot{E}_{\mathrm{D,sep}} + \dot{E}_{\mathrm{D,tur}} + \dot{E}_{\mathrm{D,reg}} + \dot{E}_{\mathrm{D,val}} + \dot{E}_{\mathrm{D,mix}} + \dot{E}_{\mathrm{D,con}} \tag{38}$$

The exergy efficiency for flue gas boosting OTEC system is

$$\eta_{\mathrm{ex}} = \frac{W_{\mathrm{net}}}{\dot{E}_{\mathrm{in}} + \dot{E}_{\mathrm{in,fg}}} \tag{39}$$

The exergy efficiency for production water boosting OTEC system is

$$\eta_{\mathrm{ex}} = \frac{W_{\mathrm{net}}}{\dot{E}_{\mathrm{in}} + \dot{E}_{\mathrm{in,hw}}} \tag{40}$$

where $\dot{E}_{\mathrm{in}}$, $\dot{E}_{\mathrm{in,fg}}$ and $\dot{E}_{\mathrm{in,hw}}$ are the input exergy from system, flue gas and production water, respectively.

The system design parameters input to model are listed in Table 2.

3.5. Model validation

The present OTEC model for predicting Kalina cycle performance is verified by the comparison of thermodynamic parameters of each state point with those in Ref. [39]. Ammonia-water (NH_3–H_2O) mixture with base liquid concentration of 0.80 is adopted as working medium. The evaporation temperature is 115 °C, the evaporation pressure is 2.17 MPa, the condensation temperature is 25 °C, and the mass flow rate is 1 kg s^{-1}. The comparison of thermodynamic parameters of each state point including the temperature, pressure, specific enthalpy, ammonia mass fraction and specific entropy are listed in Table 3. It can be found that the maximum and average relative errors are 4.75 % and 0.78 % respectively, which indicates that the present model is reliable and has high accuracy.

4. Results and discussion

4.1. Effect of flue gas waste heat quantity on system performance

Fig. 3 shows the effects of flue gas waste heat quantity ($\dot{Q}_{\mathrm{fg}}$) on performance of four systems, i.e., systems I, II, III and IV. From Fig. 3 (a), it can be seen that with the increase of $\dot{Q}_{\mathrm{fg}}$ from 2000 to 4000 kW, the power generation (W_{net}) for systems I, II, III and IV increase from 17.51 to 121.34 kW, 18.30–125.24 kW, 18.32–125.35 kW and 19.18–127.05 kW, respectively. The reason for this phenomenon is as follows. With the increase of $\dot{Q}_{\mathrm{fg}}$, the temperature of surface seawater at the inlet of evaporator rises, causing the higher evaporation temperature and mass flow rate of rich ammonia vapor ($\dot{m}_{\mathrm{v}}$). As shown in Fig. 3 (b), with the increase of $\dot{Q}_{\mathrm{fg}}$, $\dot{m}_{\mathrm{v}}$

Table 2
System design parameters input to model.

Parameters	Value
η_{tur}	0.87
η_{g}	0.9
η_{p}	0.8
η_{wp}	0.85
η_{cp}	0.85
$T_{\mathrm{c,\ in}}$	4.2 °C
ρ_{w}	1023 kg m^{-3}
ρ_{c}	1030 kg m^{-3}
V_{w}	1 m s^{-1}
V_{c}	1 m s^{-1}
L_{w}	100 m
L_{c}	1000 m
P_{a}	0.101 MPa
T_{a}	25 °C
Minimum heat exchange temperature difference in evaporator	5 °C
Minimum heat exchange temperature difference in regenerator	5 °C
Minimum heat exchange temperature difference in condenser	5 °C
Pressure drop in evaporator and regenerator	0.01 MPa
Pressure drop in condenser	0.02 MPa

Table 3
Comparison of thermodynamic parameters of each state point.

State point	Temperature/°C			Pressure/MPa			Specific enthalpy/kJ·kg^{-1}			Ammonia mass fraction			Specific entropy/kJ·kg^{-1}·K^{-1}		
	Present study	Ref. [35]	Error /%	Present study	Ref. [35]	Error /%	Present study	Ref. [35]	Error /%	Present study	Ref. [35]	Error /%	Present study	Ref. [35]	Error /%
1	42.3	42.3	0.0	2.18	2.18	0	329.6	328.0	0.48	0.80	0.80	0	1.730	1.725	0.29
2	115.0	115.0	0.0	2.17	2.17	0	1470.7	1469.9	0.05	0.80	0.80	0	4.991	4.987	0.08
3	115.0	115.0	0.0	2.17	2.17	0	1862.7	1862.5	0.01	0.95	0.95	0	6.117	6.116	0.02
4	74.8	77.5	3.4	0.81	0.81	0	1725.2	1751.6	1.51	0.95	0.95	0	6.176	6.252	1.22
5	115.0	115.0	0.0	2.17	2.17	0	450.2	429.8	4.75	0.41	0.41	0	2.059	2.036	1.13
6	54.7	53.0	3.2	2.16	2.16	0	140.6	135.0	4.15	0.41	0.41	0	1.215	1.173	3.58
7	54.9	53.2	3.2	0.81	0.81	0	140.6	135.0	4.15	0.41	0.41	0	1.219	1.178	3.48
8	71.2	72.6	1.9	0.81	0.81	0	1289.0	1307.6	1.42	0.80	0.80	0	4.808	4.865	1.17
9	25.0	25.0	0.0	0.79	0.79	0	245.2	245.2	0.00	0.80	0.80	0	1.462	1.462	0.00
10	25.2	25.2	0.0	2.19	2.19	0	247.2	247.3	0.04	0.80	0.80	0	1.462	1.462	0.00

and the enthalpy drop of rich ammonia vapor passing through steam turbine (Δh_v) both increase, causing the increase of W_{net}. Since W_{net} of system IV is highest among four systems, it has the highest thermal efficiency (η_{th}). From Fig. 3 (a), it also can be seen that with the increase of $\dot{Q}_{fg}$ from 2000 to 4000 kW, η_{th} for systems I, II, III and IV increase from 1.368 % to 6.946 %, 1.376 %–6.961 %, 1.377 %–6.996 % and 1.442 %–7.070 %, respectively.

From Fig. 3 (c), it can be seen that the exergy efficiency (η_{ex}) for four systems all increase with the increase of $\dot{Q}_{fg}$, and the growth rate of η_{ex} decreases with the increase of $\dot{Q}_{fg}$. For example, with the increase of $\dot{Q}_{fg}$ from 2000 to 2200 kW, η_{ex} is relatively increased by 42.8 %; with the increase of 3800–4000 kW, η_{ex} is relatively increased by 2.3 %. System IV has the highest η_{ex}. Since the temperature of surface seawater at the inlet of evaporator rises with the increase of $\dot{Q}_{fg}$, the exergy input to system increases. Although the total exergy destruction ($\dot{E}_{D,total}$) for four systems all increase with the increase of $\dot{Q}_{fg}$, η_{ex} for four systems still increase with the increase of $\dot{Q}_{fg}$.

4.2. Effect of production water waste heat quantity on system performance

Fig. 4 shows the effects of production water waste heat quantity ($\dot{Q}_{hw}$) on performance of four systems, i.e., systems I, II, III and IV. System I is also investigated as benchmark for comparison. For system I, $\dot{Q}_{hw}$ is 0, and the power generation (W_{net}) is fixed at 64.51 kW. From Fig. 4 (a), it can be seen that with the increase of $\dot{Q}_{hw}$ from 0 to 100 kW, W_{net} for systems II, III and IV increase from 64.51 to 69.02, 69.13 and 72.63 kW respectively, with the increment degrees are of 6.99 %, 7.16 % and 12.59 % respectively. W_{net} for system IV is larger than those of systems II and III. The difference in W_{net} among various systems are caused by mass flow rate of rich ammonia vapor ($\dot{m}_v$) and enthalpy drop of rich ammonia vapor passing through steam turbine (Δh_v). As shown in Fig. 4 (b), with the increase of $\dot{Q}_{hw}$ from 0 to 100 kW, $\dot{m}_v$ for systems II and III increase from 1.134 to 1.201 and 1.189 kg s^{-1} respectively. With the increase of $\dot{Q}_{hw}$, the temperature of surface seawater at the inlet of evaporator for system II rises, and the temperature of ammonia-water mixture base fluid for system III rises, causing the increase of $\dot{m}_v$. For system IV, due to the unchanged evaporation temperature and base fluid concentration, $\dot{m}_v$ is fixed at 1.134 kg s^{-1}; however, the waste heat of high-temperature production water causes the rich ammonia vapor to change from saturation to superheated state, thus Δh_v significantly increases with the increase of $\dot{Q}_{hw}$. Taking $\dot{Q}_{hw} = 100$ kW as an example, Δh_v for system IV is 75.99 kJ kg^{-1}, which is larger than those for system II and III (68.58 and 69.27 kJ kg^{-1}). The combining effect of $\dot{m}_v$ and Δh_v variation tendency causes W_{net} for system IV to be larger than those for systems II and III. From Fig. 4 (a), it also can be seen that the thermal efficiency (η_{th}) for system IV is higher than those for systems II and III; with the increase of $\dot{Q}_{hw}$ from 0 to 100 kW, η_{th} for systems II, III and IV are relatively increased by 0.39 %, 0.63 % and 5.72 %, respectively.

From Fig. 4 (c), it can be seen that the exergy efficiency (η_{ex}) for three systems all increase with the increase of $\dot{Q}_{hw}$, which is due to the increase of W_{net}. Taking system IV as an example, with the increase of $\dot{Q}_{hw}$ from 0 to 100 kW, η_{ex} increases from 32.20 % to 33.12 %. The total exergy destruction ($\dot{E}_{D,total}$) for three systems all increase with the increase of $\dot{Q}_{hw}$, and the increment degrees for systems II, III and IV are 9.05 %, 8.07 % and 7.71 %, respectively.

4.3. Effect of evaporation pressure on system performance

Fig. 5 shows the effects of evaporation pressure (P_{eva}) on performance of four systems. From Fig. 5 (a), it can be seen that the power generation (W_{net}) of each system rises first and then decreases with the increase of P_{eva}, meaning that an optimal P_{eva} (1.5 MPa) corresponding to the maximum W_{net}. When P_{eva} is higher than the optimal value, the decrease degrees of W_{net} for four systems are different. Taking P_{eva} rising from 1.5 to 2.0 MPa as an example, the decrease degrees of W_{net} for systems I, II, III and IV are 32.08 %, 26.68 %, 26.66 % and 23.14 %, respectively. W_{net} for system IV is largest among four systems.

From Fig. 5 (b), it can be seen that under different P_{eva}, the mass flow rate of rich ammonia vapor ($\dot{m}_v$) follows the order of system II > system III > system IV = system I. With the increase of P_{eva}, $\dot{m}_v$ for each system decreases. The reason for this phenomenon is that the increase of P_{eva} results in the decrease of mass flow rate of ammonia-water mixture base fluid and then the decrease of evaporated ammonia. Meanwhile, the enthalpy drop of rich ammonia vapor passing through steam turbine (Δh_v) increases with the in-

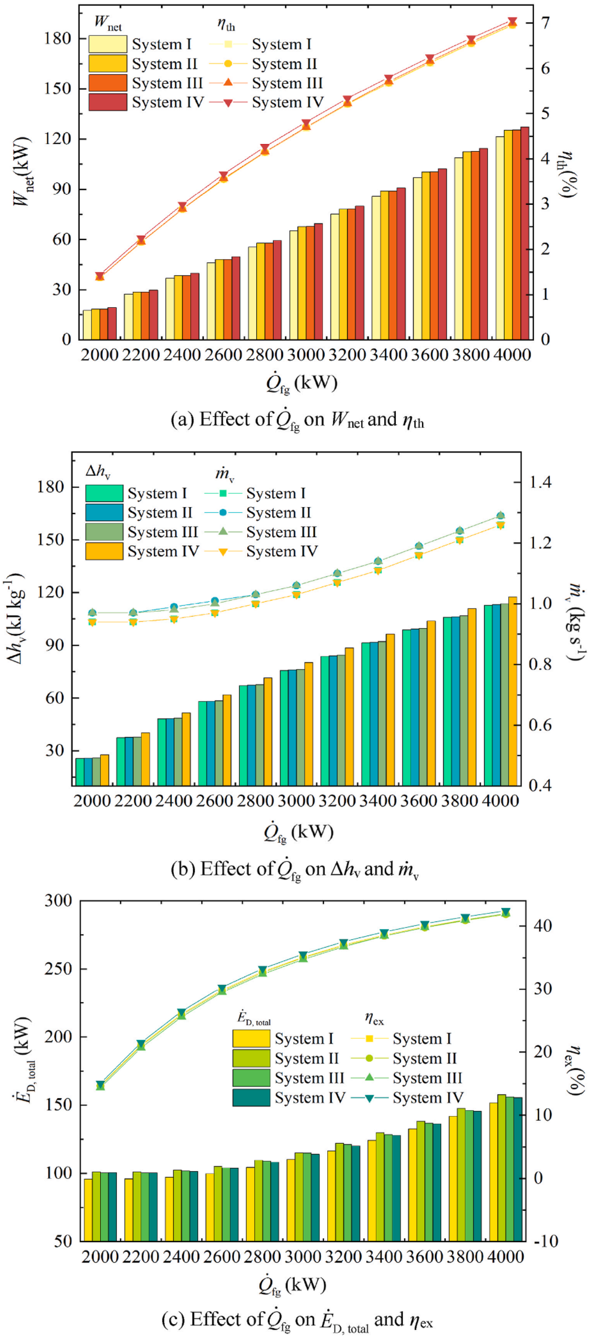

Fig. 3. Effects of flue gas waste heat quantity ($\dot{Q}_{fg}$) on system performance.

crease of P_{eva}, and the growth rate decreases with the increase of P_{eva}. Taking system I as an example, Δh_v is increased by 22.77 kJ kg^{-1} with the increase of P_{eva} from 1.0 to 1.2 MPa, while is increased by 9.94 kJ kg^{-1} with the increase of P_{eva} from 1.8 to 2.0 MPa. For lower P_{eva}, the increment degree of Δh_v is larger, and its effect on power generation is dominant, thus, W_{net} of each system rises first with the increase of P_{eva}. For higher P_{eva}, the increment degree of Δh_v is smaller, and the effect of q_v on power generation is dominant, thus, W_{net} of each system decreases with the increase of $P_{eva.}$ For system IV, the waste heat of high-temperature production water causes the rich ammonia vapor to change from saturation to superheated state, thus Δh_v for system IV is much larger than those for other three systems. Taking $P_{eva} = 2.0$ MPa as an example, Δh_v for systems I, II, III and IV are 104.24, 104.96, 105.49 and 125.41 kJ kg^{-1}, respectively. Therefore, W_{net} for system IV is largest among four systems under different P_{eva}.

From Fig. 5 (a), it can be seen that the thermal efficiency (η_{th}) of each system increases with the increase of P_{eva}, which is inconsistent with the variation tendency of W_{net}. This phenomenon is caused by the following reason. With the increase of P_{eva}, the total heat

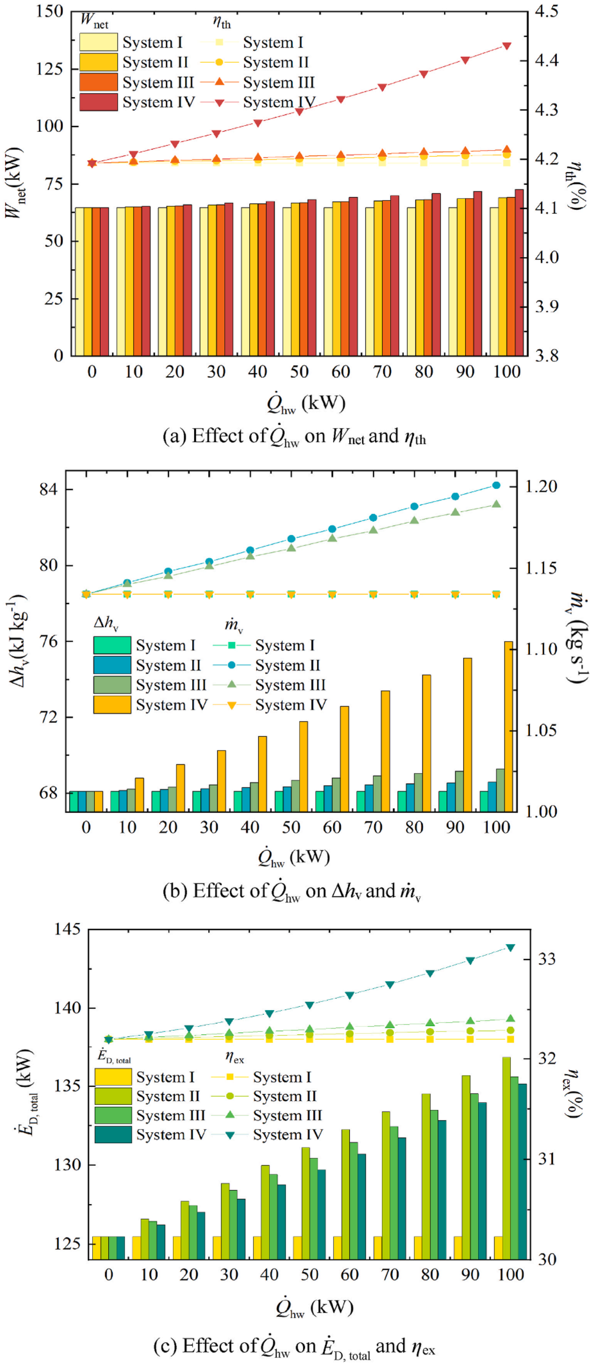

(a) Effect of $\dot{Q}_{hw}$ on W_{net} and η_{th}

(b) Effect of $\dot{Q}_{hw}$ on Δh_v and $\dot{m}_v$

(c) Effect of $\dot{Q}_{hw}$ on $\dot{E}_{D, total}$ and η_{ex}

Fig. 4. Effects of production water waste heat quantity ($\dot{Q}_{hw}$) on system performance.

input to system decreases, although W_{net} starts to decrease at higher P_{eva}, η_{th} is always increased. For P_{eva} less than 1.3 MPa, the difference of η_{th} among four systems is slight; with the increase of P_{eva}, η_{th} for system IV is significantly higher than those for other three systems. From Fig. 5 (c), it can be seen that the variation tendency of exergy efficiency (η_{ex}) is consistent with that of η_{th}. The total exergy destruction ($\dot{E}_{D,total}$) decreases with the increase of P_{eva}, indicating that the higher P_{eva} is beneficial to the utilization of energy.

4.4. Effect of base fluid concentration on system performance

Fig. 6 shows the effects of base fluid concentration (x_b) on performance of four systems. From Fig. 6 (a), it can be seen that the power generation (W_{net}) of each system rises first and then decreases with the increase of x_b, meaning that an optimal x_b ($x_{b, opt}$ = 0.82) corresponding to the maximum W_{net}. W_{net} for system IV is largest among four systems. For lower x_b, the difference of

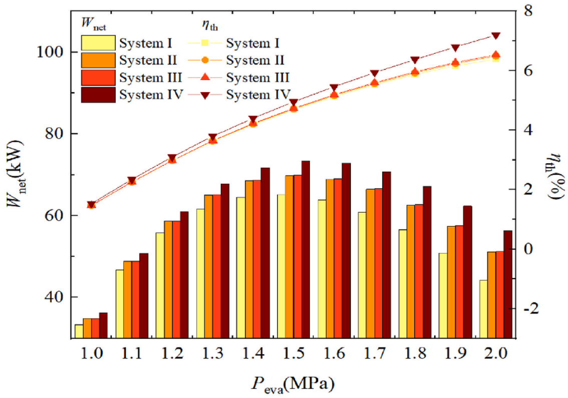

(a) Effect of P_{eva} on W_{net} and η_{th}

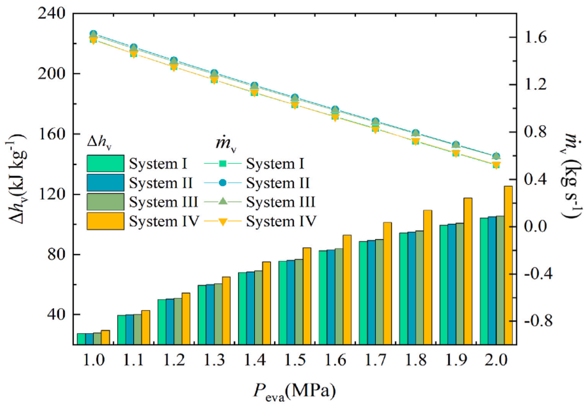

(b) Effect of P_{eva} on Δh_v and $\dot{m}_v$

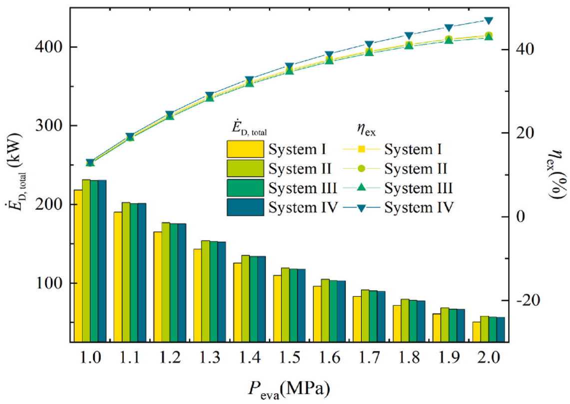

(c) Effect of P_{eva} on $\dot{E}_{D,\,total}$ and η_{ex}

Fig. 5. Effects of evaporation pressure (P_{eva}) on system performance.

W_{net} between system IV and other three systems is large; with the increase of x_b, the difference decreases gradually. For example, at $x_b = 0.70$, the differences of W_{net} between system IV and systems I, II and III are is 9.64, 4.62 and 4.56 kW, respectively; at $x_b = 0.90$, the differences are 5.61, 2.24 and 1.93 kW, respectively. With the increase of x_b, the thermal efficiency (η_{th}) for each system decreases gradually, which is caused by the increase of heat exchange quantity in evaporator.

From Fig. 6 (b), it can be seen that with the increase of x_b, the mass flow rate of rich ammonia vapor ($\dot{m}_v$) for each system increases. $\dot{m}_v$ for system II is largest among four systems, which is due to its highest evaporation temperature and largest amount of released ammonia. The enthalpy drop of rich ammonia vapor passing through steam turbine (Δh_v) decreases with the increase of $x_{b.}$ The reason for this phenomenon is as follows. The increase of x_b results in the increase of condensation pressure at the fixed condensation

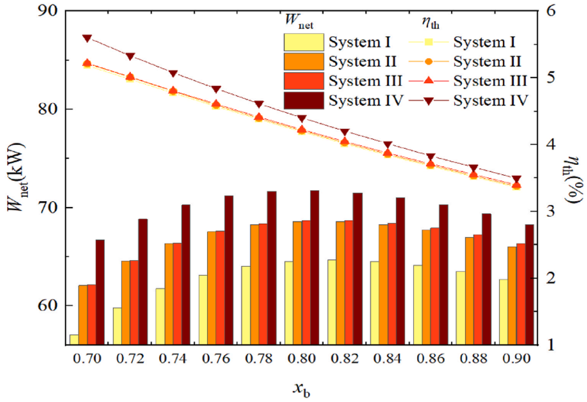

(a) Effect of x_b on W_{net} and η_{th}

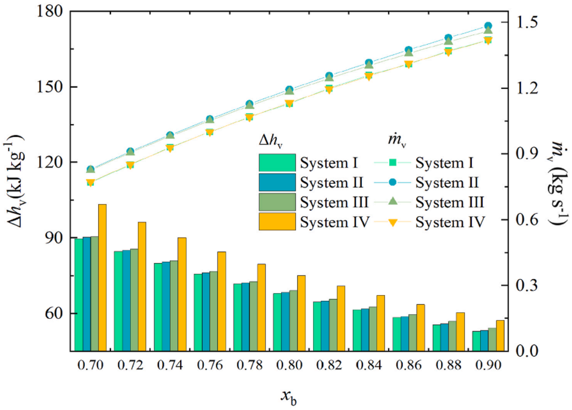

(b) Effect of x_b on Δh_v and $\dot{m}_v$

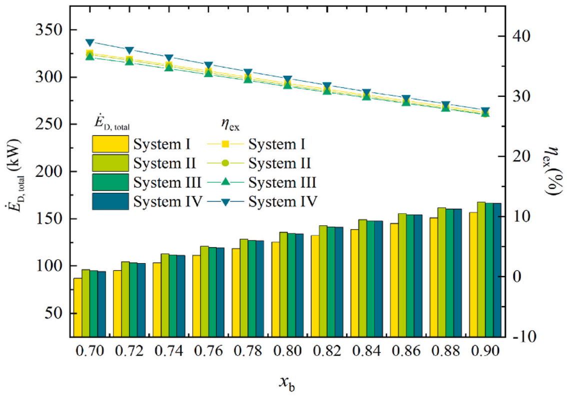

(c) Effect of x_b on $\dot{E}_{D, total}$ and η_{ex}

Fig. 6. Effects of base fluid concentration (x_b) on system performance.

temperature and the increase of steam turbine outlet pressure, causing the decrease of Δh_v. The combining effect of $\dot{m}_v$ and Δh_v leads to the variation tendency of W_{net}.

From Fig. 6 (c), it can be seen that with the increase of x_b, the exergy efficiency (η_{ex}) of each system gradually decreases and the total exergy destruction ($\dot{E}_{D,total}$) continuously increases. When x_b increases from 0.70 to 0.90, η_{ex} for systems I, II, III and IV are decreased by 26.52 %, 26.71 %, 26.06 % and 29.10 %, respectively. As the auxiliary heat source for system II is used to heat the surface seawater not entering the evaporator, the exergy input from the auxiliary heat source will lead to the increase of exergy destruction for all components of system, thus, $\dot{E}_{D,total}$ for system II is larger than those for other three systems.

4.5. *Effect of condensation temperature on system performance*

Fig. 7 shows the effects of condensation temperature (T_{con}) on performance of four systems. From Fig. 7 (a), it can be seen that with the increase of T_{con}, the power generation (W_{net}) and thermal efficiency (η_{th}) of each system both decrease. When T_{con} rises from

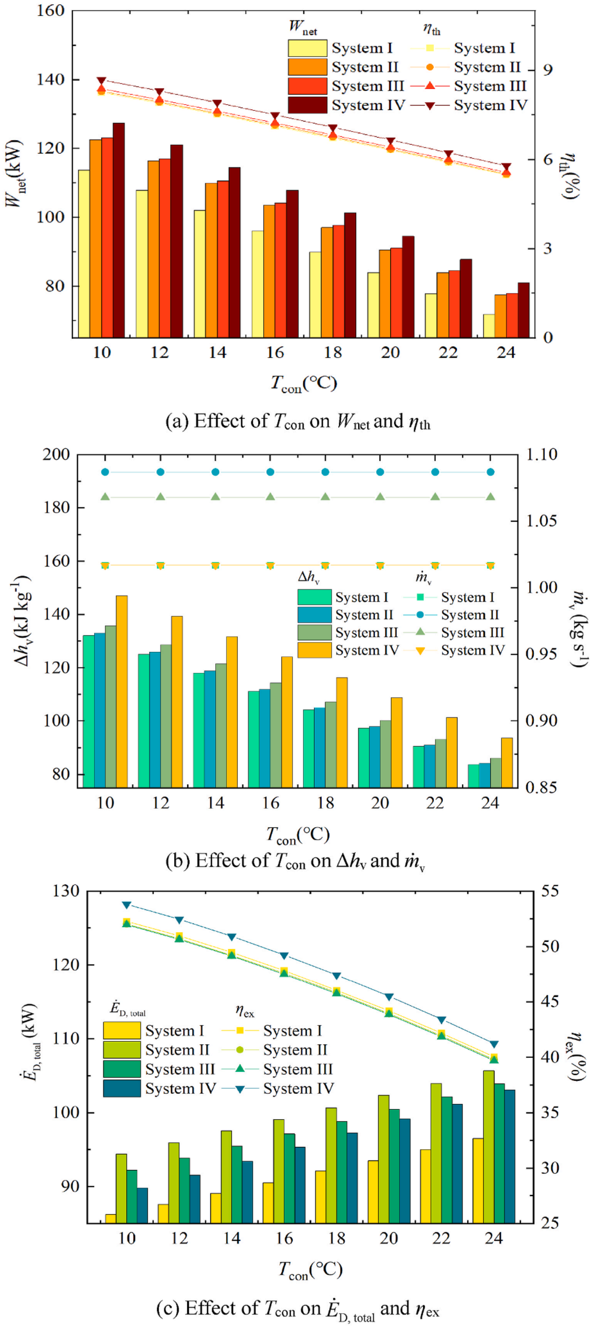

Fig. 7. Effects of condensation temperature (T_{con}) on system performance.

10 to 24 °C, for systems I, II, III and IV, W_{net} are decreased by 36.88 %, 36.83 %, 36.76 % and 36.38 % respectively, η_{th} are decreased by 33.63 %, 33.61 %, 33.56 % and 33.31 % respectively. At different T_{con}, W_{net} and η_{th} for system IV are higher than those for other three systems. The reason for the decrease of W_{net} is as follows. The increase of T_{con} causes the increase of condensation pressure, which leads to the increase of pressure at steam turbine outlet and then the decrease of enthalpy drop of rich ammonia vapor passing through steam turbine (Δh_v), as shown in From Fig. 7 (b). Meanwhile, the mass flow rate of rich ammonia vapor ($\dot{m}_v$) is not affected by T_{con}.

From Fig. 7 (c), it can be seen that with the increase of T_{con}, the exergy efficiency (η_{ex}) of each system decreases and the total exergy destruction ($\dot{E}_{D,total}$) increases. When T_{con} rises from 10 to 24 °C, for systems I, II, III and IV, η_{ex} are decreased by 23.40 %, 23.53 %, 23.64 % and 23.35 %, respectively. This phenomenon is caused by the following reason. The increase of T_{con} leads to the increase of exergy destruction of condenser and then the increase of $\dot{E}_{D,total}$, while W_{net} decreases with the increase of T_{con}, which results in the decrease of η_{ex} with the increase of T_{con}.

4.6. Comparison of system performance

Based on the above analysis, it can be seen that system IV has larger power generation (W_{net}), thermal efficiency (η_{th}) and exergy efficiency (η_{ex}) than systems I, II and III. This phenomenon is caused by the following reasons. For system IV, the rich ammonia vapor is changed from saturation to superheated state due to the waste heat of high-temperature production water, causing the enthalpy drop of rich ammonia vapor passing through steam turbine (Δh_v) for system IV to be larger than those for other three systems. As the waste heat quantity is fixed, the thermal efficiency (η_{th}) and exergy efficiency (η_{ex}) for system IV are also higher than those for other three systems. In order to disclose the influence of waste heat recovery from offshore oil and gas platform on OTEC system performance, the performance comparison between system IV and single OTEC system are performed, as shown in Fig. 8. The evaporation pressure (P_{eva}) is 1 MPa, the base fluid concentration (x_b) is 0.80, and the condensation temperature (T_{con}) is 24 °C. The waste heat quantity of high-temperature flue gas ($\dot{Q}_{fg}$) is 3000 kW, and the waste heat quantity of high-temperature production water ($\dot{Q}_{hw}$) is 50 kW. Compared with single OTEC system, for system IV, W_{net}, η_{th} and η_{ex} increase from 2.43 to 40.56 kW, 2.26 %–3.85 %, 6.25 %–14.89 % respectively, with the increment degrees of 1569.13 %, 70.35 % and 138.26 % respectively. The reason for this phenomenon is as follows. The waste heat of high-temperature flue gas and production water are adopted to heat the surface seawater and rich ammonia vapor respectively, which increases the mass flow rate of rich ammonia vapor and enthalpy drop of rich ammonia vapor passing through steam turbine, thereby improving W_{net}, η_{th} and η_{ex}.

5. Conclusions

This paper proposed a novel ocean thermal energy conversion system integrated with waste heat recovery from offshore oil and gas platform (OTEC-WHROG). According to the waste heat sources (high-temperature flue gas and production water) and heated objects, four systems are designed, including flue gas boosting OTEC system (system I), production water boosting surface seawater OTEC system (system II), production water boosting working medium OTEC system (system III), and production water boosting vapor OTEC system (system IV). The effects of flue gas waste heat quantity, production water waste heat quantity, evaporation pressure, base fluid concentration and condensation temperature on system performance are investigated, and compared with single OTEC system. The following conclusions could be drawn.

(1) The power generation (W_{net}), thermal efficiency (η_{th}) and exergy efficiency (η_{ex}) for four systems all increase with the increase of flue gas waste heat quantity ($\dot{Q}_{fg}$). W_{net}, η_{th} and η_{ex} for system IV are larger than those for other three systems. For system IV, with the increase of $\dot{Q}_{fg}$ from 2000 to 4000 kW, the increment degrees of W_{net}, η_{th} and η_{ex} are 562 %, 390 % and 181 % respectively. W_{net}, η_{th} and η_{ex} for systems II, III and IV all increase with the increase of production water waste heat quantity ($\dot{Q}_{fg}$). W_{net}, η_{th} and η_{ex} for system IV are larger than those for other two systems. For system IV, with the increase of $\dot{Q}_{fg}$ from 0 to 100 kW, the increment degrees of W_{net}, η_{th} and η_{ex} are 12.59 %, 5.73 % and 2.86 % respectively.

(2) For four systems, W_{net} rises first and then decrease with the increase of evaporation pressure (P_{eva}) or base fluid concentration (x_b), presenting an optimal P_{eva} of 1.5 MPa and x_b of 0.82 corresponding to the maximum W_{net}; W_{net} decreases with the increase of condensation temperature (T_{con}); η_{th} and η_{ex} increase with the increase of P_{eva}, decrease with the increase of x_b, and decrease with the increase of T_{con}.

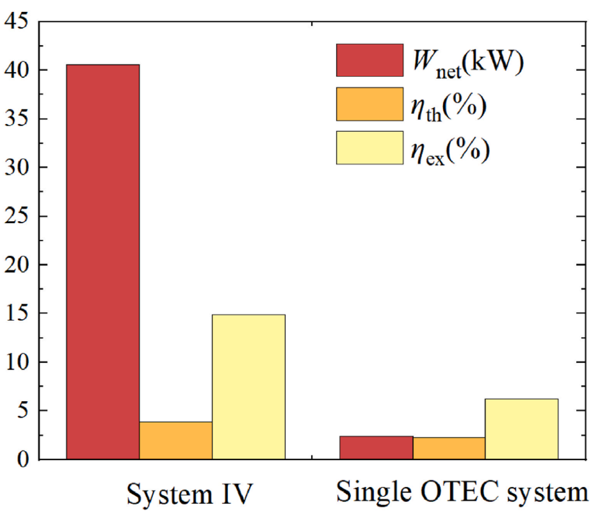

Fig. 8. Performance comparison between system IV and single OTEC system.

(3) System IV has larger W_{net}, η_{th} and η_{ex} than other three systems. Compared with single OTEC system, for system IV, W_{net}, η_{th} and η_{ex} are increased by 1569.13 %, 70.35 % and 138.26 %, respectively.

CRediT authorship contribution statement

Yanlian Du: Validation, Software, Methodology, Investigation. **Hao Peng:** Writing – review & editing, Writing – original draft, Conceptualization. **Jiahua Xu:** Validation, Software, Methodology, Investigation. **Zhen Tian:** Writing – review & editing. **Yuan Zhang:** Writing – review & editing. **Xuanhe Han:** Writing – review & editing. **Yijun Shen:** Writing – review & editing.

Declaration of competing interest

The authors declare that they have no known competing financial interests or personal relationships that could have appeared to influence the work reported in this paper.

Data availability

The authors do not have permission to share data.

Acknowledgements

The authors gratefully acknowledge the support from The National Natural Science Foundation of China (Key Program, Grant No. 52231012), Hainan Province Science and Technology Special Fund (Grant No. ZDYF2020207), State Key Laboratory of Marine Resource Utilization in South China Sea (Hainan University) (Grant No. MRUKF2023015), and Start-up Research Foundation of Hainan University (Grant No. KYQD(ZR)-22059).

References

[1] J.P. Peng, Y.Z. Ge, F.Y. Chen, L. Liu, H.Y. Wu, W.M. Liu, Theoretical and experimental study on the performance of a high-efficiency thermodynamic cycle for ocean thermal energy conversion, Renew. Energy 185 (2022) 734–747.
[2] J. Langer, J. Quist, K. Blok, Recent progress in the economics of ocean thermal energy conversion: critical review and research agenda, Renew. Sustain. Energy Rev. 130 (2020) 109960.
[3] H. Aydin, H.S. Lee, H.J. Kim, S.K. Shin, K. Park, Off-design performance analysis of a closed-cycle ocean thermal energy conversion system with solar thermal preheating and superheating, Renew. Energy 72 (2014) 154–163.
[4] L. Aresti, P. Christodoulides, C. Michailides, T. Onoufriou, Reviewing the energy, environment, and economy prospects of Ocean Thermal Energy Conversion (OTEC) systems, Sustain. Energy Technol. Assessments 60 (2023) 103459.
[5] K. Rajagopalan, G.C. Nihous, Estimates of global Ocean Thermal Energy Conversion (OTEC) resources using an ocean general circulation model, Renew. Energy 50 (2013) 532–540.
[6] J.Y. Jung, H.S. Lee, H.J. Kim, Y. Yoo, W.Y. Choi, H.Y. Kwak, Thermoeconomic analysis of an ocean thermal energy conversion plant, Renew. Energy 86 (2016) 1086–1094.
[7] C.C. Fan, Z. Wu, J.D. Wang, Y.P. Chen, C.B. Zhang, Thermodynamic process control of ocean thermal energy conversion, Renew. Energy 210 (2023) 810–821.
[8] M. Kolahi, M. Yari, S.M.S. Mahmoudi, F. Mohammadkhani, Thermodynamic and economic performance improvement of ORCs through using zeotropic mixtures: case of waste heat recovery in an offshore platform, Case Stud. Therm. Eng. 8 (2016) 51–70.
[9] R. Agathokleous, G. Bianchi, G. Panayiotou, L. Arestia, M.C. Argyrou, G.S. Georgiou, S.A. Tassou, H. Jouhara, S.A. Kalogirou, G.A. Florides, P. Christodoulides, Waste Heat Recovery in the EU industry and proposed new technologies, Energy Proc. 161 (2019) 489–496.
[10] S.Y. Teng, M.W. Wang, H. Xi, S.Q. Wen, Energy, exergy, economic (3E) analysis, optimization and comparison of different ORC based CHP systems for waste heat recovery, Case Stud. Therm. Eng. 28 (2021) 101444.
[11] R. Zhar, A. Allouhi, A. Jamil, K. Lahrech, A comparative study and sensitivity analysis of different ORC configurations for waste heat recovery, Case Stud. Therm. Eng. 28 (2021) 101608.
[12] U.R. Kelem, F. Yilmaz, Development and assessment of a novel multigeneration plant combined with a supercritical CO_2 cycle for multiple products, Int. J. Hydrogen Energy 52 (2024) 1306–1318.
[13] A.I. Kalina, Combined-cycle system with novel bottoming cycle, J. Eng. Gas Turbines Power 106 (1984) 737–742.
[14] X.X. Zhang, M.G. He, Y. Zhang, A review of research on the Kalina cycle, Renewable Sustainable Energy Rev. 16 (2012) 5309–5318.
[15] C.E.C. Rodríguez, J.C.E. Palacio, O.J. Venturini, E.E.S. Lora, V.M. Cobas, D. Marques dos Santos, F.R.L. Dotto, V. Gialluca, Exergetic and economic comparison of ORC and Kalina cycle for low temperature enhanced geothermal system in Brazil, Appl. Therm. Eng. 52 (2013) 109–119.
[16] A. Nemati, H. Nami, F. Ranjbar, M. Yari, A comparative thermodynamic analysis of ORC and Kalina cycles for waste heat recovery: a case study for CGAM cogeneration system, Case Stud. Therm. Eng. 9 (2017) 1–13.
[17] W.M. Liu, X.J. Xu, F.Y. Chen, Y.J. Liu, S.Z. Li, L. Liu, Y. Chen, A review of research on the closed thermodynamic cycles of ocean thermal energy conversion, Renewable Sustainable Energy Rev. 119 (2020) 109581.
[18] H. Uehara, Y. Ikegami, T. Nishida, Performance Analysis of OTEC system using a cycle with absorption and extraction process, Trans. Jpn. Soc. Mech. Eng. B 64 (1998) 384–389.
[19] W.M. Liu, F.Y. Chen, Y.Q. Wang, W.J. Jiang, Progress of closed-cycle OTEC and study of a new cycle of OTEC, Adv. Mater. Res. 354–355 (2012) 275–278.
[20] J.I. Yoon, C.H. Son, S.M. Baek, B.H. Ye, H.J. Kim, H.S. Lee, Performance characteristics of a high-efficiency R717 OTEC power cycle, Appl. Therm. Eng. 72 (2014) 304–308.
[21] H. Yuan, N. Mei, P.L. Zhou, Performance analysis of an absorption power cycle for ocean thermal energy conversion, Energy Convers. Manag. 87 (2014) 199–207.
[22] E. Kusuda, T. Morisaki, Y. Ikegami, Performance test of double-stage Rankine cycle experimental plant for OTEC, Procedia Eng. 105 (2015) 713–718.
[23] J.I. Yoon, S.H. Seol, C.H. Son, S.H. Jung, Y.B. Kim, H.S. Lee, H.J. Kim, J.H. Moon, Analysis of the high-efficiency EP-OTEC cycle using R152a, Renew. Energy 105 (2017) 366–373.
[24] Z.X. Wu, H.J. Feng, L.G. Chen, W. Tang, J.C. Shi, Y.L. Ge, Constructal thermodynamic optimization for ocean thermal energy conversion system with dual-pressure organic Rankine cycle, Energy Convers. Manag. 210 (2020) 112727.
[25] N.J. Kim, S.H. Shin, W.G. Chun, A study on the thermodynamic cycle of OTEC system, Journal of the Korean Solar Energy Society 26 (2006) 9–18.
[26] N.J. Kim, K.C. Ng, W. Chun, Using the condenser effluent from a nuclear power plant for Ocean Thermal Energy Conversion (OTEC), Int. Commun. Heat Mass Tran. 36 (2009) 1008–1013.
[27] N. Yamada, A. Hoshi, Y. Ikegami, Performance simulation of solar-boosted ocean thermal energy conversion plant, Renew. Energy 34 (2009) 1752–1758.
[28] P. Ahmadi, I. Dincer, M.A. Rosen, Energy and exergy analyses of hydrogen production via solar-boosted ocean thermal energy conversion and PEM Electrolysis,

Int. J. Hydrogen Energy 38 (2013) 1795–1805.
[29] N. Arcuri, R. Bruno, P. Bevilacqua, LNG as cold heat source in OTEC systems, Ocean Engineering 104 (2015) 349–358.
[30] N.H.M. Idrus, M.N. Musa, W.J. Yahya, A.M. Ithnin, Geo-Ocean thermal energy conversion (GeOTEC) power cycle/plant, Renew. Energy 111 (2017) 372–380.
[31] F. Yilmaz, Energy, exergy and economic analyses of a novel hybrid ocean thermal energy conversion system for clean power production, Energy Convers. Manag. 196 (2019) 557–566.
[32] F. Yilmaz, M. Ozturk, R. Selbas, Thermodynamic performance assessment of ocean thermal energy conversion based hydrogen production and liquefaction process, Int. J. Hydrogen Energy 43 (2018) 10626–10636.
[33] X.L. Liu, G.C. Gong, Y. Wu, H.X. Li, Thermal performance analysis of Brayton cycle with waste heat recovery boiler for diesel engines of offshore oil production facilities, Appl. Therm. Eng. 107 (2016) 320–328.
[34] M.M.L. Reis, J.A.V. Guillen, W.L.R. Gallo, Off-design performance analysis and optimization of the power production by an organic Rankine cycle coupled with a gas turbine in an offshore oil platform, Energy Convers. Manag. 196 (2019) 1037–1050.
[35] L. Pierobon, T.V. Nguyen, U. Larsen, F. Haglind, B. Elmegaard, Multi-objective optimization of organic Rankine cycles for waste heat recovery: application in an offshore platform, Energy 58 (2013) 538–549.
[36] H. Nami, I.S. Ertesvåg, R. Agromayor, L. Riboldi, L.O. Nord, Gas turbine exhaust gas heat recovery by organic Rankine cycles (ORC) for offshore combined heat and power applications - energy and exergy analysis, Energy 165 (2018) 1060–1071.
[37] L. Pierobon, A. Benato, E. Scolari, F. Haglind, A. Stoppato, Waste heat recovery technologies for offshore platforms, Appl. Energy 136 (2014) 228–241.
[38] L. Pierobon, F. Haglind, Design and optimization of air bottoming cycles for waste heat recovery in off-shore platforms, Appl. Energy 118 (2014) 156–165.
[39] J.Y. Meng, Analysis and Optimization on the Kalina Cycle in Low-Temperature. Master Thesis, Tianjin University, 2014 (in Chinese).